

RESEARCH ARTICLE

Validation of the Beddoes–Leishman dynamic stall model for horizontal axis wind turbines using MEXICO data

Ricardo Pereira¹, Gerard Schepers² and Marilena D. Pavel¹

¹ Faculty of Aerospace Engineering, Delft University of Technology, Delft 2629 HS, The Netherlands

² Department of Wind Energy, Energy Research Centre (ECN), Petten 1755 LE, The Netherlands

ABSTRACT

The aim of this study is to assess the load predicting capability of a classical Beddoes–Leishman dynamic stall model in a horizontal axis wind turbine environment, in the presence of yaw misalignment. The dynamic stall model was tailored to the horizontal axis wind turbine environment and validated against unsteady thick airfoil data. Subsequently, the dynamic stall model was implemented in a blade element-momentum code for yawed flow, and the results were compared with aerodynamic measurements obtained in the MEXICO (Model Rotor Experiments under Controlled Conditions) project on a wind turbine rotor placed in a large scale wind tunnel. In general, reasonable to good agreement was found between the blade element-momentum model and MEXICO data. When large yaw misalignments were imposed, poor agreement was found in the downstroke of the movement between the model and the experiment. Still, over a revolution, the maximum normal force coefficient predicted was always within 8% of experimental data at the inboard stations, which is encouraging especially when blade fatigue calculations are being considered. Copyright © 2012 John Wiley & Sons, Ltd.

KEYWORDS

HAWT; dynamic stall; Beddoes–Leishman; MEXICO

Correspondence

Ricardo Pereira, Faculty of Aerospace Engineering, Delft University of Technology, Delft 2629 HS, The Netherlands.

E-mail: asimov1984@gmail.com

Received 17 February 2011; Revised 9 September 2011; Accepted 7 October 2011

NOMENCLATURE

b	semichord, m
c	chord, m
$C_{L,0}$	potential lift coefficient
$C_{l,2D}$	two-dimensional lift coefficient
$C_{l,3D}$	three-dimensional lift coefficient
$C_{d,2D}$	two-dimensional drag coefficient
$C_{d,3D}$	three-dimensional drag coefficient
C_n	normal force coefficient
$C_{n,I}$	critical normal force coefficient
$C_{n,MAX}$	maximum normal force coefficient
$C_{n,MEXICO}$	normal force coefficient from the MEXICO experiment
D	diameter, m
$F_{n,Interp}$	normal force obtained with pressure sensor interpolation, N
k	reduced frequency
M	Mach number
$P_{MAX,Interp}$	maximum pressure interpolation, Pa
r	local radius, m
R	radius, m
Re	Reynolds number
U	wind speed, m s^{-1}

V	flow velocity, m s^{-1}
T_p, T_f, T_v, T_{vl}	Beddoes–Leishman dynamic time constants
y	airfoil ordinate, m
α	angle of attack, deg
α_{LEsep}	leading-edge separation angle of attack, deg
β	yaw-misalignment angle, deg
$\varepsilon_{C_n, \text{Avg}}$	normal coefficient average relative error
$\varepsilon_{C_n, \text{MAX}}$	relative error in maximum normal force coefficient
θ_{tw}	twist angle, deg
Ψ	azimuth angle, deg
Ω	revolution frequency, rad s^{-1}
ω	frequency, rad s^{-1}

1. INTRODUCTION

Horizontal axis wind turbines (HAWT) operate most of their time in an adverse, unsteady aerodynamic environment that is both hard to define using measurements and also to predict using mathematical models.^{1–3} As described in Leishman,³ ‘the airloads on each blade element may vary in time because the turbine is often yawed with respect to the oncoming wind, and also because of shear in the ambient wind, ambient turbulence, blade flapping and vibratory displacements, and other factors such as tower shadow.’ For wind turbines, the issues associated with flow unsteadiness are particularly acute. For example,³ compared with helicopters, large wind turbines have relatively low rotor rpm and corresponding low tip speeds (about 3–5 s per rotor revolution). This denotes that changes in wind speed or atmospheric perturbations can result in significant changes in blade element angle of attack (AoA). Also, when the turbine is yawed with respect to the wind, there are large fluctuations in the relative velocity at the profile’s leading edge (LE). These large amplitude oscillations in local AoA and onset velocity contribute significantly to the unsteady flow environment on the wind turbine blades.

Dynamic stall (DS) is a significant unsteady flow problem taking place on rotary wings (helicopters and wind turbines). Generally, an airfoil experiences DS when two conditions are met: (i) large enough reduced frequency and (ii) large values of AoA, larger than that of static stall. For the same AoA range, DS is known to impose large load amplitude on the airfoil section, when compared with the static loading characteristic. DS is expected to occur in HAWT operation, especially when yaw misalignment is present, and consequentially, it becomes crucial to predict the load magnitudes DS will impose on the blades.

The unsteadiness associated with the flow field and the turbine operating state is usually quantified by the reduced frequency k . The reduced frequency is defined as the ratio of the physical frequency of the flow ω , multiplied by blade chord c and the average flow velocity V , i.e. $k \stackrel{\text{def}}{=} \omega b/V = \omega c/2V$. The factor 2 in the expression was introduced by historical reasons.* According to Leishman⁴, one can consider that if $k < 0.05$ the problem is quasi-steady, i.e. the unsteady effects are generally small and can be neglected; if a problem is characterized by a reduced frequency $k > 0.05$, it is considered unsteady, and the unsteady terms in the equations cannot be neglected if a realistic analysis is to be conducted. When $k > 0.2$, the unsteady terms will begin to dominate the behaviour of the airloads, and consequentially, the problem is highly unsteady. For a HAWT, if the induction velocities are neglected, the average blade section flow velocity V is $V = U_{\text{eff}} = \sqrt{(\Omega r)^2 + U^2}$ where Ω is the rotor rpm, r is the local blade radius and U is the wind speed.

In a yaw-misaligned wind turbine, one may expect that the flow in a given rotating blade section will have a periodic behaviour over time, with identical characteristics obtained for similar azimuthal positions. In other words, this means that the dominant frequency of excitation in a yaw-misaligned wind turbine matches the angular frequency of the blade’s rotation, i.e. $\omega = \Omega$, which is usually also termed 1P or 1/rev. Noticing that the incoming wind speed U is small in magnitude when compared with the rotational speed Ωr , one can assume that the magnitude of the local effective velocity U_{eff} a blade element will experience is given by the in-plane velocity component, i.e. $V = \Omega r$. Thus, the reduced frequency of a yaw-misaligned wind turbine can be approximated as $k \approx \Omega c/2\Omega r = c/2r$, showing that reduced frequency depends on the local blade chord to radius ratio that is usually referred to as local solidity in wind turbine terminology. Typical values of the discussed variables found in wind turbine blades are given in Table I.

Looking at the values of the reduced frequencies in Table I, it is possible to see that for wind turbines, reduced frequencies k in the range 0.035 to 0.12 are present, which means mostly unsteady character problems. It should also be mentioned that in wind engineering, it is commonly considered that a reduced frequency greater than 0.02 results in unsteady effects;⁶ this benchmark is somewhat smaller than the value indicated by Leishman,⁴ but wind tunnel experiments with pitch oscillating airfoils show some hysteresis even when such low frequency excitations are imposed.

*The original work of Theodorsen⁵ on airfoil unsteady aerodynamics used the profile’s semichord as length scale.

Table I. Typical reduced frequencies for wind turbine operations.

r/R	c/r	$k(1P)$
0.3	0.25	0.12
0.5	0.15	0.075
0.75	0.07	0.035

Usually, the unsteady effects taking place in wind turbine aerodynamics can be divided into three ‘contributions’:⁷

- *Dynamic inflow* is an inviscid effect on the induced velocity, usually caused by a change in blade pitch angle or in rotor speed. It has a time scale in the order of D/U , where D stands for the diameter of the rotor and U represents the incoming wind velocity.
- The *Theodorsen* effect is also of non-viscous nature, and it refers to the change on the airfoil characteristics while in fully attached flow conditions, namely the delay of the airloads with respect to the AoA when it varies rapidly. This effect has a time scale in the order of c/V_{Eff} , where c stands for the airfoil’s chord and V_{Eff} represents the effective local velocity.
- *Dynamic stall* is a viscous effect on the airfoil characteristics at stalled conditions that yields large magnitude transient forces, involving a rather complex set of interlinked phenomena; it is also characterized by a time scale in the order of c/V_{Eff} .

In HAWT’s normal operating regimes, the two time scales of the unsteady effects mentioned above, D/U and c/V_{Eff} , will have very different orders of magnitude, and consequentially, it is usual to study the effects of dynamic inflow and the airfoil unsteady aerodynamics separately.

2. MODELLING DYNAMIC STALL FOR WIND TURBINES

The mechanism of DS was first identified on helicopters. The importance of unsteady aerodynamics was considered in Harris and Pruyn,⁸ when helicopter design engineers were unable to predict the performance of high-speed helicopters using conventional aerodynamics. For a good review of DS research associated with helicopters, the reader is referred to Leishman,⁴ Crimi and Yaggy,⁹ McCroskey¹⁰ and Carr and Lawrence.¹¹ Many typical engineering models developed to predict the effects of DS on helicopters are a form of re-synthesis of the measured unsteady airfoil airloads, simply ‘rebuilding’ the trends observed experimentally. On the other hand, there are semi-empirical models that contain simplified representations of the physical processes taking place by using sets of linear and non-linear equations to simulate the aerodynamic loads. Some of the classic models developed to predict DS effects in helicopters that may be suitable for rotor airloads prediction are as follows: UTRC α , A, B method,^{11,12} Boeing-Vertol ‘gamma’ function method,¹³ time delay method,^{14,15} Gangwani’s method,¹⁶ Johnson’s method,¹⁷ Beddoes–Leishman’s method¹⁸ and ONERA method.¹⁹ As stated previously, these DS models contain a re-synthesis of measured unsteady airfoil airloads and try to ‘rebuild’ experimental trends in a semi-empirical form by using a number of empirical parameters, usually both from steady and unsteady experiments, to capture the physics of DS phenomenon. Therefore, their application is limited to the airfoil and Mach number they are developed.

In a wind turbine, the characteristic airflow may significantly differ from other types of rotating machines (such as helicopters), since the normal operating regime Mach number and rotational frequency will be considerably lower; moreover, the airfoils used in wind turbine blades are usually thicker. Consequentially, some of the DS models mentioned previously were adapted to wind turbine environment (such as ONERA method²⁰). Specific DS engineering models ‘tuned’ for wind turbines have been developed, namely Øye,²¹ Larsen–Nielsen–Krenk,²² ECN Model,²³ Sheng–Galbraith–Coton²⁴ and Gupta.²⁵ However, all these adaptations were related to comparisons with 2D airfoil measured data. To the authors’ best knowledge, there is no reference adapting the Beddoes–Leishman model to full-scale wind turbine data.

Schepers²⁶ compared experimental data from a yaw-misaligned turbine with a blade element momentum (BEM)-like model, which used ECN DS model²³ to account for the DS effects, but the results obtained indicated that including the DS model did not improve the BEM model’s performance.

2.1. Beddoes–Leishman dynamic stall model overview

The original Beddoes–Leishman DS method¹⁸ is capable of assessing the unsteady lift, pitching moment and drag, giving a physical representation of the unsteady aerodynamic problem. The method has been extensively validated with experimental data.¹⁸ It is composed of three subsystems: an attached flow model for the unsteady linear airloads, a separated flow model for the non-linear airloads and a DS model for the airloads induced by the LE vortex. The loads in the attached flow

regime are obtained through indicial functions, where compressibility is taken into account; for the aerodynamic effects associated with separated flow, the Beddoes–Leishman method calculates an dynamic equivalent point of separation on the basis of the static or quasi-static condition according to Kirchhoff/Helmholtz theory and the AoA history, which is then used to reconstruct the non-linear loads; finally, the dynamic effects of a concentrated LE vortex passing across the upper surface and being convected downstream are taken into account to represent the DS effects. This method assumes that the DS process is initiated when an equivalent LE pressure parameter reaches a critical value. This method yields indeed quite good results, and it has the important advantage that it requires relatively few empirical coefficients, most of which derived from static airfoil data; this explains why it is so popular and has been extensively used in helicopter rotor loads prediction.

In the present paper, it was chosen to implement the semi-empirical Beddoes–Leishman model¹⁸ and adapt it to the HAWT environment. One can thus expect the unsteady airfoil aerodynamic physical phenomena to be simulated while keeping the amount of empirical ‘tuning’ parameters to a reasonably simple degree.

3. METHODOLOGY

3.1. Adapting the Beddoes–Leishman dynamic stall model for wind turbine applications

The Beddoes–Leishman DS model was originally developed for helicopter applications, and consequentially, it includes the effects of the air’s compressibility. In a HAWT environment, the expected Mach numbers of operation are $M < 0.3$; accordingly, in this study, the DS model was simplified by assuming *incompressible flow*. Another major difference between helicopter and HAWTs is the airfoil sections used. Usually, the profiles for HAWT applications are thick, with relative thicknesses larger than 15%, whereas helicopter blades are normally equipped with thinner airfoil sections. According to Leishman and Beddoes,¹⁸ the most critical aspect of DS modelling is to predict the occurrence of LE separation. In the original Beddoes–Leishman DS model, LE separation is assumed to take place when a certain critical normal force coefficient, $C_{n,I}$, is attained. This value can be obtained from the airfoil’s static characteristic by taking the normal force coefficient at which a break in the pitching moment curve is visible.

However, when thick airfoils are considered, usually significant trailing-edge separation takes place before LE separation occurs. Accordingly, the normal force coefficient may decrease with increasing AoA before the break in the pitching moment curve occurs. This means that using the criterion from Leishman and Beddoes,¹⁸ the critical normal force coefficient obtained may actually correspond to a value lower than the maximum C_n , which is unrealistic. In thick airfoils’ static aerodynamic data, it can also happen that no clear break is visible in the pitching moment versus AoA curve.

Consequentially, it is clear that a different criterion to compute the critical normal force coefficient is needed for HAWT airfoil sections.

3.1.1. Leading-edge separation criteria.

In this paper, two different *LE separation criteria* were implemented in the DS model. The first approach was based on the work of Timmer *et al.*,²⁷ where the LE separation AoA is related with the LE thickness. In his work, Timmer *et al.* obtained a linear empirical relation based on wind tunnel testing for several thick airfoils, expressed in degrees:

$$\alpha_{LEsep} = 1170.8 \frac{y}{c} - 1.33 \quad (1)$$

In the expression, the nose thickness is represented by the y/c ordinate, obtained at a relative chordwise position of 1.25%. The critical normal coefficient is then calculated assuming

$$C_{n,I} = (2\pi\alpha_{LEsep} + C_{L,0}) \cos \alpha_{LEsep} \quad (2)$$

The second approach used to compute the critical normal force coefficient simply takes the maximum value of the normal force coefficient, i.e.

$$C_{n,I} = C_{n,MAX} \quad (3)$$

The Ohio State University database²⁸ of unsteady measurements was used to compare the implemented criteria. Thick airfoils were selected for comparison, and the reduced frequencies of excitation were chosen to be representative of what one expects to find in a yaw-misaligned HAWT. Some results are shown in the following figures.

In Figures 1 and 2, it is clear that the $C_{n,MAX}$ criterion yielded a better agreement with experimental data than the Timmer criterion. Experimental data obtained with other airfoils and at other reduced frequencies also compared better with the $C_{n,MAX}$ criterion, and consequentially, it was used in subsequent calculations.

It should also be mentioned that in Figure 2, as well as in results obtained with other thick airfoils and at different reduced frequencies,²⁹ an abrupt decay of the normal force coefficient can be observed in the experimental data. This indicates that LE separation occurs, which is also hinted by abrupt changes in the pitching moment verified in the OSU data.

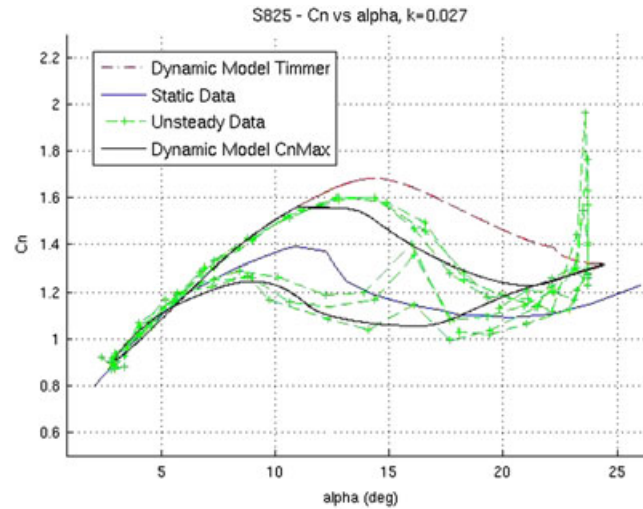


Figure 1. Dynamic stall model results obtained at low reduced frequency ($k = 0.027$).

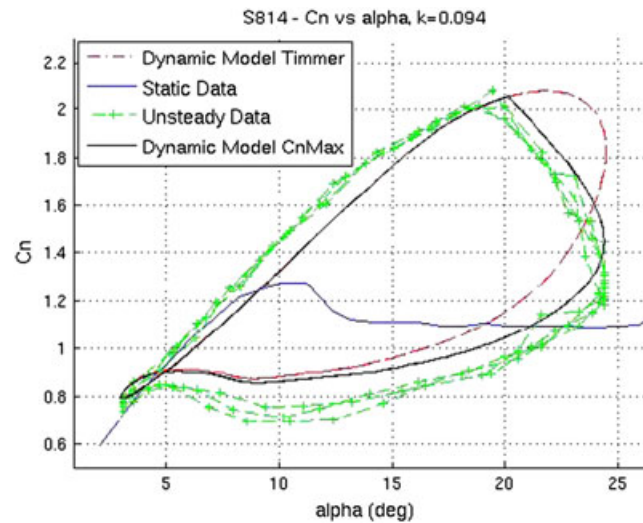


Figure 2. Dynamic stall model results obtained at high reduced frequency ($k = 0.094$).

Consequently, it seems unrealistic to disregard LE separation on HAWT application airfoils based simply on the fact that the aerodynamic sections are thick.

3.1.2. Empirical time constants.

It was mentioned previously that the Beddoes–Leishman DS model uses empirical time constants to account for the time delay in aerodynamic loading the airfoil will experience, with respect to the static characteristic. The values of these time constants will obviously have a large impact on the load predictions, since they directly affect the dynamics of the unsteady model. In this study, it was chosen to select a set of ‘reference’ values for these empirical constants.

The time constants related with the unsteady *attached flow* are insensitive to the Mach number and airfoil section’s shape and consequentially were simply taken from Leishman and Beddoes.¹⁸ However, when there is *flow separation*, the choice of the time constants becomes more delicate. In Leishman and Beddoes,¹⁸ it is indicated that the time constants associated with the pressure lag and with the vortex lift, T_p and T_v , respectively, are *mainly dependent* of the *Mach number*, and not so much of the airfoil shape. As for the viscous lag T_f , the same reference indicates that this parameter is sensitive *both* to *profile geometry* and *Mach number*.

In the current study, the values of the empirical time constants were selected by making use of two sources:

- The original Beddoes–Leishman DS model refers to a document from *Westland Helicopters*,³⁰ in which empirical time constants are given for the NACA0012 airfoil on the basis of unsteady experiments at $Re = 8 \times 10^6$ and for Mach numbers as low as 0.3.
- The Swedish Aeronautical Research Institute or FFA conducted an optimization of the empirical time constants in a Beddoes–Leishman DS model³¹ by comparing load predictions with experimental data for several thick, wind turbine airfoils at low Mach numbers. ‘Reference’ values were put forward, which yielded reasonable agreement for the majority of the considered airfoils. However, this Beddoes–Leishman DS model implementation does not use a criterion for the start of ‘vortex travelling’, assuming that *no LE separation* takes place, on the basis of the fact that wind turbine application airfoils are thick.

Taking that into account, the values of the empirical time constants in the current implemented model were selected as follows. For the *peak pressure lag time constant* T_p , it was chosen to follow the trend of decreasing Mach number from Leishman and Beddoes³⁰ as plotted in Figure 3, also because in Mert³¹ a ‘reference’ value for this time constant was not clearly indicated. Regarding the *boundary layer lag time constant* T_f , the ‘reference’ value from Mert³¹ was used, since this parameter is sensitive to airfoil shape; consequentially, it makes little sense to use the value specifically derived for a (thin) profile from Mert.³¹ As for the time constants related to the *vortex lift*, it was again chosen to follow the trend of decreasing Mach number from Leishman and Beddoes,³⁰ since the DS model implemented in Mert³¹ did not consider vortex shedding. The trend observed in Westland’s empirical time constants with decreasing Mach number is shown in Figure 3, where a cubic spline extrapolation was used for the low Mach numbers.

One should also notice that the influence of the Mach number on different spanwise stations was assumed negligible, since the local Mach number is always below 0.3. Consequentially, the same set of time constants was used for all spanwise stations.

The set of parameters from the references mentioned previously are indicated in Table II, together with the values used in the current implementation:

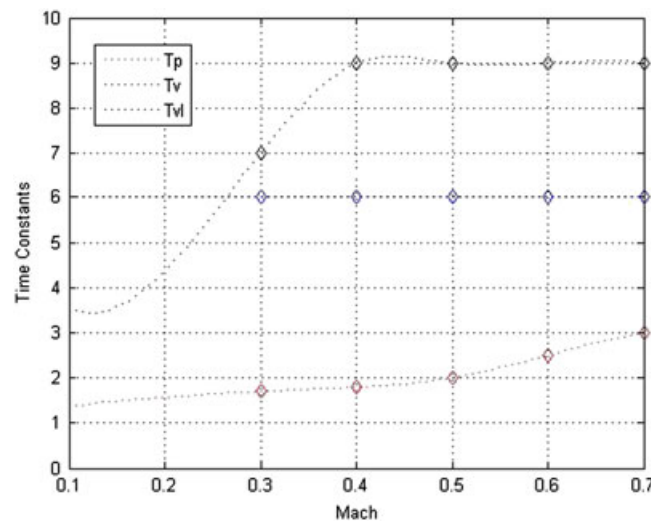


Figure 3. Trend of Westland time constants.

Table II. Values of the empirical time constants for separated flow.

Time constant	T_p [1/s]	T_f [1/s]	T_v [1/s]	T_{vl} [1/s]
Westland ($M = 0.3$) ³⁰	1.7	3	6	7
FFA ('Reference') ³¹	0.8	5	2	—
Implemented model	1.5	5	6	5

3.2. Implementation in the blade element momentum code

Distinct modelling approaches have been used in the past to simulate the aerodynamics of a HAWT rotor. BEM theory can be considered simple, and it has been derived several decades ago; but still, it is used in present days, mostly but not only in preliminary stages of HAWT design. Other more complex approaches include actuator line theory³² and vortex wake theory,³³ both computationally very consuming. Actuator line theory solves full 3D Reynolds Averaged Navier–Stokes equations around the HAWT rotor and introduces the rotating blade forces contribution through source terms along lines representing the blades. These blade forces are determined iteratively, which obviously can lead to prohibitive computing times especially if DS phenomena are present. As for vortex wake methods, they assume the Kutta condition to be met; given the fact that one is interested in thick airfoils operating at high angles of attack, significant LE separation is to be expected; consequentially, circulation should no longer be assumed to vary linearly with the AoA. Having this in mind, it was chosen to implement the DS model in a BEM code.

Considering rotary wings, BEM theory states that the variation of the momentum of the air particles in the cylinder containing the rotor disc is equal to the aerodynamic forces on the blades. In HAWTs, the blades will act to slow down the incoming wind, and it is common to express this velocity change by means of induced velocities or induction factors:

$$U_R = U_0(1 - \alpha) \quad (4)$$

where U_R is the wind speed at the rotor plane and U_0 represents the unperturbed wind speed. The induction factors are usually represented by α and are normally calculated iteratively.

When yaw misalignment is present, the induced velocities will change with radial and azimuthal position, and there is no simple theory that accurately describes this velocity distribution. The BEM code used in the present study used an **empirical model** for the induced axial velocities from Schepers *et al.*³⁴ Even though there are also induced tangential velocities, the present BEM model does not take them into account, on the basis of the fact that these should be of a much smaller magnitude than the axially induced velocities. This ‘empirical’ BEM code was used since previous work²⁹ showed that it performed better than a ‘classical’ BEM code, i.e. than the approach suggested in classical HAWT aerodynamic literature such as Burton *et al.*³⁵

3.2.1. Radial dependency of sectional aerodynamic coefficients.

The effect of stall delay at inboard stations in rotary wings, usually termed rotational augmentation, has long been documented.³⁶ Spanwise stations near the blade root usually operate at large angles of attack and will experience large AoA amplitudes when yaw misalignments are present. Since one wishes to assess performance of a DS model, particularly at inboard stations, it is thus fundamental to include the rotational augmentation on the aerodynamic coefficients.

For the lift coefficient, the correction of Snel³⁶ was implemented into the model:

$$C_{l,3D} = C_{l,2D} 3 \left(\frac{c}{r} \right)^2 \Delta C_l \quad (5)$$

where c/r is the ratio between the local chord and the local radius, and ΔC_l represents the difference between the static airfoil characteristic and the potential lift coefficient.

For the drag coefficient, the correction of Chaviaropoulos and Hansen³⁷ was used:

$$C_{d,3D} = C_{d,2D} + 2.2 \left(\frac{c}{r} \right) \cos^4(\theta_{tw}) \Delta C_d \quad (6)$$

where θ_{tw} is the local blade twist angle and ΔC_d is the difference between the 2D drag coefficient and the drag coefficient obtained when the AoA is zero.

On the basis of Chaviaropoulos and Hansen³⁷ and Pereira,²⁹ both lift and drag corrections were applied up to an AoA of 25°, after which the correction itself was decreased linearly to zero at an AoA of 60°. Also, both corrections were only applied from the root of the blade up to a spanwise position of 50%, i.e. up to the radial coordinate $r/R = 0.5$. For further information, the reader is referred to Pereira.²⁹

Figure 4 illustrates how the complete model computes the sectional aerodynamic coefficients:

3.2.2. Discretization and convergence of the model.

The model was run considering an *azimuthal increment of 10° and 15 elements in the spanwise direction*. This level of discretization was imposed since previous work²⁹ showed that it was sufficient to capture the trends relevant for DS phenomena.

To run the computational model, initial values of the aerodynamic history parameters (LE vortex position, dynamic trailing-edge separation point, etc) must be prescribed to the DS method, which means that some iteration time must be allowed before the model reaches a definite solution. Previous work²⁹ showed that after one blade revolution, the load

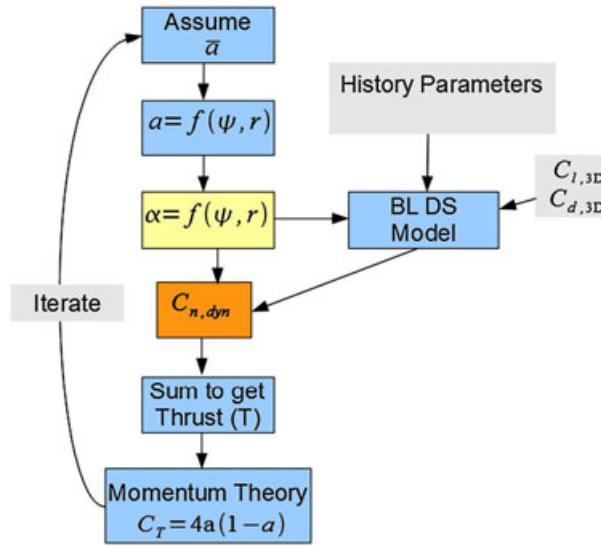


Figure 4. Complete blade element momentum model diagram.

predictions are no longer influenced by the initial condition imposed; consequentially, the computational results obtained for the 3rd blade revolution were used for comparison with experimental data.

3.2.3. Experimental data used for comparison.

The MEXICO (Model Rotor Experiments under Controlled Conditions) experiment was performed within a project developed by the European Union with the main goal of providing a database of aerodynamic measurements of a HAWT. The project started in January 2001 and ended in December 2006, when an extensively instrumented 4.5 m diameter HAWT model was tested in the German-Dutch Wind Tunnel under several flow conditions. Table III illustrates the experiment.

The MEXICO rotor was equipped with 148 pressure sensors with a sampling frequency of 5.5 kHz, distributed over five spanwise stations. Flatwise and bendwise moments were measured at the root of the blade with strain gauges, and also stereo Particle Image Velocity measurements were made in the rotor plane and further downstream. In this study, the results obtained with the complete BEM model are validated against MEXICO data, using the *normal force coefficient* for comparison. The experimental force coefficient was computed from the MEXICO pressure measurements. A *cubic interpolation* of the *pressure* measured by each sensor* was performed over the airfoil surface, and this pressure distribution was integrated over a cubic interpolation of the airfoil surface, yielding the *normal force*. To obtain the normal force coefficient,† the computed forces were divided by the maximum pressure occurring over the airfoil, taken as the *maximum of the cubic interpolation* of the pressure sensors, multiplied by the local chord, according to

$$C_{n,MEXICO} = \frac{F_{n,Interp}}{c \cdot P_{max,Interp}} \quad (7)$$


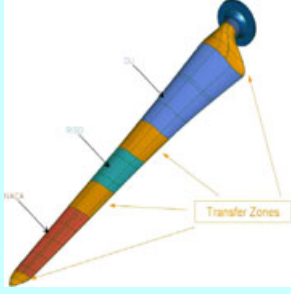
Dynamic stall phenomena are expected to occur mostly at *inboard sections*, since at these spanwise stations usually larger angles of attack are found, and yaw misalignments will cause large AoA variations over a revolution. Consequentially, emphasis is given at the 25 and 35% spanwise stations of the MEXICO data.

When a wind turbine rotor is not aligned with the incoming wind, the rotating blades will be advancing or retreating with respect to the non-aligned wind component. This will originate an oscillation in the in-plane velocity component, which leads to a cyclic AoA variation over a blade revolution, usually termed advancing/retreating blade effect.²⁶ In the MEXICO yawed configuration, this effect imposes a minimum AoA at the vertically downward azimuthal position, which in the current study corresponds to $\Psi = 180\text{deg} \rightarrow \alpha_{min}$, and maximum incidence at the vertically upward angular coordinate, $\Psi = 0\text{deg} \rightarrow \alpha_{max}$. Since this effect will be dominant at the inboard stations when large wind speeds are considered,

*It should be noted that the pressure measured by each sensor in the MEXICO rotor blades is the gauge pressure, i.e. the pressure relatively to the atmospheric pressure.

†These are section force coefficients, i.e. per metre span; thus, the maximum pressure in the denominator should be multiplied by the local chord of the airfoil.

Table III. The MEXICO experiment.

	Upstream Velocity [m/s]	{5; 10; 15; 18; 24; 30}
	Yaw Angle [°]	{−30; 0; 15; 30; 45}
	Rotor Speed [rpm]	{0; 324.5; 424.5}
	Pitch Angle [°]	[−5, 3; 90]
	Blade Airfoils	DU91-W2-250 (25%max thickness) @ r/R [0.2;0.5] RISOE a1-21 (21%max thickness) @ r/R [0.5;0.7] NACA64418 (18%max thickness) @ r/R [0.7;1]

the *upstroke* of the cycle, i.e. the period when the AoA is increasing, corresponds to *azimuthal positions from 180 to 360°*. By analogy, the *downstroke* of the cycle, i.e. the period when the AoA is decreasing, corresponds to **azimuthal positions from 0 to 180°**.

4. RESULTS AND DISCUSSION

The azimuthal variation of the normal force coefficients obtained experimentally and with the computational model is now presented. The normal force coefficient's variation with the AoA is also shown. To assess the influence of the DS model, the results obtained without the DS model are also displayed.

It was chosen to compare the computational model with experimental results obtained at a wind tunnel speed of 24 m s^{-1} because at this large wind speed, DS phenomena are expected to occur. Figures 5–8 show the C_n and AoA variations as a function of the azimuth-imposing moderate and large yaw angles, $\beta = [30; 45]^\circ$. The angles of attack expected to occur during the experiments are also indicated in Table IV.

Generally speaking, reasonable to good agreement was found between the predicted loading and the MEXICO data. Including the DS model in the BEM code improves the load prediction capability when compared with the static BEM, especially when large angles of attack are imposed. When considering large yaw misalignments, the agreement found is not so good; in the downstroke motion, measurements seem to indicate that significant separation occurs, whereas the implemented model does not capture this trend. However, quite good agreement was found in the upstroke motion, and consequently, the amplitude of the loading over a revolution is well predicted.

The performance of the implemented calculation method is qualitatively assessed by computing the *average relative error* in the *normal force coefficient* obtained with BEM code including the DS model. The magnitude of the error was calculated by averaging the relative error of model results over a revolution and assuming the MEXICO data to be the exact solution:

$$\varepsilon_{C_n, \text{Avg}} = \frac{1}{360} \sum_{\Psi=1}^{360} \frac{|C_{n, \text{Model}}(\Psi) - C_{n, \text{MEXICO}}(\Psi)|}{C_{n, \text{MEXICO}}(\Psi)} \quad (8)$$

The results are shown in Table V for several MEXICO trials. The wind tunnel speed is referred to as U , and the relative error was calculated for several spanwise positions, with the result given in percentage. It should be noted that the number of experimental data points used for comparison is small and that ideally one would validate the current model with more

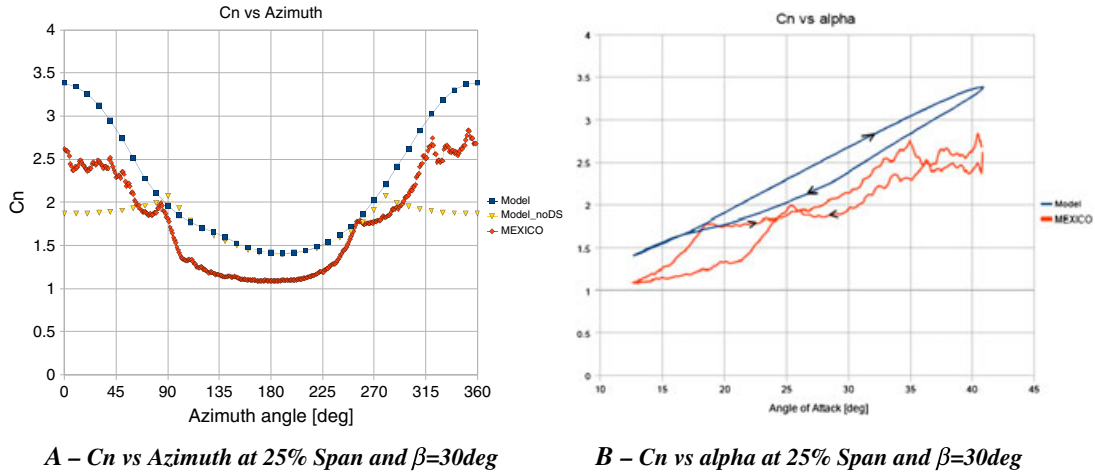


Figure 5. (a) C_n versus azimuth at 25% span and $\beta = 30^\circ$. (b) C_n versus alpha at 25% span and $\beta = 30^\circ$.

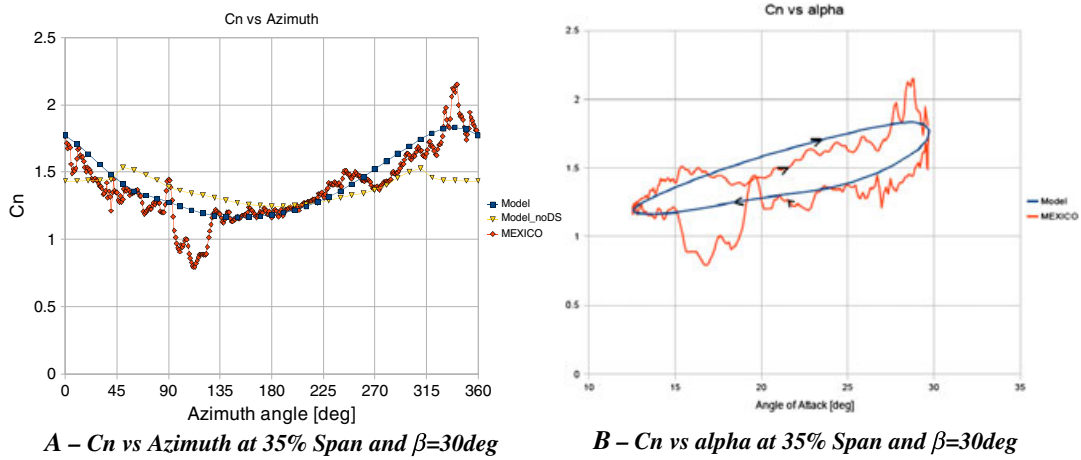


Figure 6. (a) C_n versus azimuth at 35% span and $\beta = 30^\circ$. (b) C_n versus alpha at 35% span and $\beta = 30^\circ$.

experimental data. However, and although the MEXICO experiment provided a large HAWT aerodynamic database, only few cases were suited for comparison with the present model:

The figures included before show good agreement between the predicted and experimental loading during the upstroke of the movement, even when large yaw misalignments are imposed. Since the extreme loads occurring over a revolution are important in assessing the blade's robustness and fatigue resistance, the *relative error in the maximum normal force coefficient* over a revolution was computed, according to

$$\varepsilon_{C_n, \text{MAX}} = \frac{|C_{n, \text{MEXICO}, \text{MAX}} - C_{n, \text{Model}, \text{MAX}}|}{C_{n, \text{MEXICO}, \text{MAX}}} \quad (9)$$

The results are shown in Table VI for several MEXICO trials, with the error given in percentage:

The average error in the predicted loads over a revolution is approximately 12%, except for the 25% spanwise station. However, the predicted maximum normal force coefficient occurring over a revolution was within 10% of the measured values. Specifically considering the inboard stations, where the DS influence is larger, the accuracy obtained in predicting the maximum C_n was, in average, below 8%.

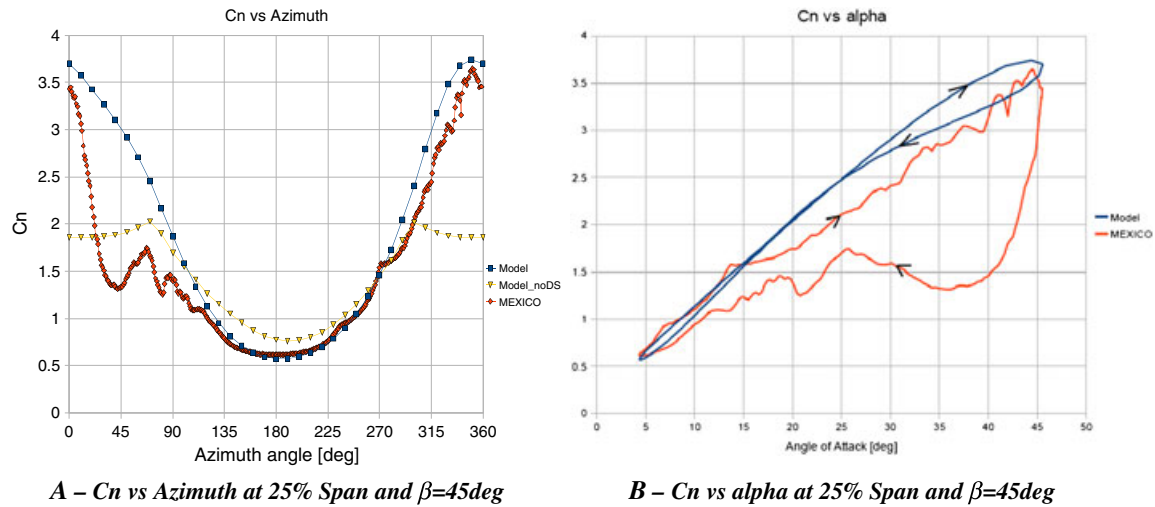


Figure 7. (a) C_n versus azimuth at 25% span and $\beta = 45^\circ$. (b) C_n versus alpha at 25% span and $\beta = 45^\circ$.

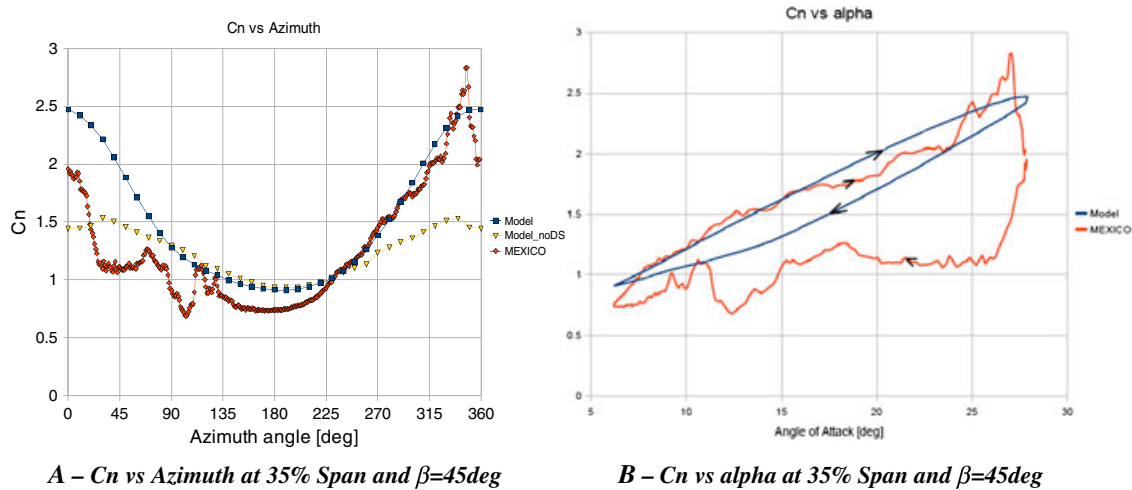


Figure 8. (a) C_n versus azimuth at 35% span and $\beta = 45\text{deg}$. (b) C_n versus alpha at 35% span and $\beta = 45^\circ$.

Table IV. Angle of attack range in MEXICO yawed configurations from Pereira.²⁹

$\alpha[\text{deg}]$	$\beta = 30$	$\beta = 45$
25% span	13–42	4–46
35% span	13–29	6–28

Table V. Average relative error in C_n over a revolution.

Trial	U (m s ⁻¹)	β (deg)	25% Span	35% span	60% span	82% span
152	18	30	12.1	8.1	12.3	10.3
153	24	30	25.4	7.6	6.5	17.9
160	24	15	12.3	11.1	9.9	14.0
167	24	45	25.1	24.0	14.5	6.4
Average	—	—	18.7	12.7	11.6	12.2

Table VI. Relative error in the maximum Cn over a revolution.

Trial	U (m s ⁻¹)	β (deg)	25% span	35% span	60% span	82% span
152	18	30	2.0	0.2	9.9	5.9
153	24	30	19.1	15.0	0.1	2.2
160	24	15	5.0	2.4	14.9	1.1
167	24	45	2.5	12.8	13.5	4.2
Average	—	—	7.2	7.6	9.6	3.4

5. CONCLUSION

Modern megawatt scale HAWTs are usually pitch controlled, meaning that stall is less likely to occur than in stall controlled machines. Nevertheless, given the size of large HAWTs, DS may occur due to the presence of yaw misalignment, gusts and atmospheric turbulence or because of the atmospheric boundary layer.

Accurate prediction of DS phenomena on HAWT blades is extremely important since extreme loading may lead to structural damage. In this study, the Beddoes–Leishman DS model was tailored for HAWT application and implemented in a BEM code. The computational results obtained in a yawed configuration were compared with experimental data from the MEXICO project. This experimental data are particularly suited for this study since the full scale HAWT model was heavily instrumented and tested under several flow regimes.

Rotational augmentation and DS are complex phenomena that are intrinsically related, but their effects have been superimposed in the current model. Still the results indicate that even though the experimental trends were not always captured, the *magnitude of the loading amplitude* occurring over a revolution in a yawed configuration at high wind speeds was well predicted. This is important, also for large scale HAWTs, especially when blade fatigue calculations are being considered and is an encouraging result.

The BEM method used is simple, and the DS model itself is not very complex. In the past, more sophisticated DS models have been put forward such as that of Sheng *et al.*;²⁴ however, it is worth investigating how to implement and integrate DS modelling in global simulation of HAWT aerodynamics. In yawed operation, the reduced frequency that an airfoil section is working at is usually estimated using 1P as excitation source. Still, one can argue that the local degree of unsteadiness is related with the time derivative of the AoA, which is related also with the yaw angle and wind speed magnitude. In future research, DS models could perhaps be validated experimentally for very high reduced frequencies, which might occur when large yaw misalignments are present.

ACKNOWLEDGEMENTS

R. Pereira would like to thank the ECN for the financial support and also the help of several ECN colleagues during the development of this research.

REFERENCES

1. Huyer SA, Simms DA, Robinson MC. Unsteady aerodynamics associated with a horizontal-axis wind turbine. *AIAA Journal* 1996; **34**(7): 1410–1419.
2. Robinson MC, Galbraith RA, Shipley D, Miller M. Unsteady aerodynamics of wind turbines, *33rd Aerospace Sciences Meeting*, Paper 95-0526, Reno, NV, January 1995.
3. Leishman JG. Challenges in modeling the unsteady aerodynamics of wind turbines, *21st ASME Wind Energy Symposium*, Reno, NV, January 14–17, 2002. AIAA-2002-0037.
4. Leishman JG. *Principles of Helicopter Aerodynamics*. Cambridge University Press: Cambridge, UK, 2006.
5. Theodorsen T. General theory of aerodynamic instability and the mechanism of flutter, 1935. *NACA-496*.
6. Snel H. Lecture on dynamic stall modeling. ECN 31/06/2009.
7. Snel H, Schepers JG. Engineering models for dynamic inflow phenomena. *Journal of Wind Engineering and Industrial Aerodynamics* 1992; **39**: 267–281.
8. Harris FD, Pruyn RR. Blade stall-half fact, half fiction. *Journal of the American Helicopter Society* April 1968; **13**(2): 49–55.
9. Crimi P, Yaggy PF. Dynamic stall. *AGARDograph no.172*, November 1973.
10. McCroskey WJ. The phenomenon of dynamic stall. March 1981. NASA Technical Memorandum.
11. Carr LW. Progress in analysis and prediction of dynamic stall. *Journal of Aircraft* Jan. 1998; **25**(1): 6–17.

12. Bielawa R. Synthesized unsteady airfoil data with applications to stall flutter calculations, 31st Annual Forum of the *American Helicopter Society*, 1975.
13. Gormont R. A mathematical model of unsteady aerodynamics and radial flow for application to helicopter rotors. *USAAVLABS TR 72-67*, 1973.
14. Beddoes T. A synthesis of unsteady aerodynamic effects including stall hysteresis. *Vertica* 1976; **1**: 113–123.
15. Beddoes T. Onset of leading edge separation effects under dynamic conditions and low Mach number, Proceedings of the 34th Annual Forum of the *American Helicopter Society*, 1978.
16. Gangwani S. Synthesized airfoil data method for prediction of dynamic stall and unsteady airloads. *Vertica* 1984; **8**: 93–118.
17. Johnson W. Comparison of Three methods for calculation of helicopter rotor blade loading and stresses due to stall. *NASA TN D-7833*, 1974.
18. Leishman J, Beddoes T. A semi-empirical model for dynamic stall. *Journal of the American Helicopter Society* 1989; **34**: 3–17.
19. Truong V. Prediction of helicopter rotor airloads based on physical modelling of 3D unsteady aerodynamics, *22nd European Rotorcraft Forum*, 1996.
20. Rapin M, Ortun B. 3D rotational correction in ONERA aeroelastic predictions of NREL wind turbine, *45th AIAA Aerospace Sciences Meeting and Exhibit*, 2007.
21. Øye S. Dynamic stall simulated as time lag of separation. *Technical report*, Department of Fluid Mechanics, Technical University of Denmark, 1991.
22. Larsen J, Nielsen S, Krenk S. Dynamic stall model for wind turbine airfoils. *Journal of Fluids and Structures* 2007; **23**(7): 959–982.
23. Snel H. Application of a modified Theodorsen model to the estimation of aerodynamic forces and aeroelastic stability, *European Wind Energy Conference*, London, 22–25 November 2004.
24. Sheng W, Galbraith R, Coton F. A modified dynamic stall model for low Mach numbers. *Journal of Solar Energy Engineering* 2008; **130**: 031013-1–031013-10.
25. Gupta S, Leishman JG. Dynamic stall modelling of the S809 aerofoil and comparison with experiments. *Wind Energy Wiley* 2006; **9**: 521–547.
26. Schepers JG. IEA annex XX: comparison between calculations and measurements on a wind turbine in yaw in the NASA-Ames windtunnel. *ECN-E-07-072*, 2007.
27. Timmer W, van Rooij R. Some aspects of high angle-of-attack flow on airfoils for wind turbine application, *European Wind Energy Conference and Exhibition*, Copenhagen, July 2001.
28. http://wind.nrel.gov/OSU_data/data/ on Jan 2010.
29. Pereira R. *Validating the Beddoes–Leishman dynamic stall model in the HAWT environment*, Msc Thesis, TUDelft, 2010.
30. Leishman J, Beddoes T. A generalised model for airfoil unsteady aerodynamic behaviour and dynamic stall using the indicial method, 42nd Annual Forum of the *American Helicopter Society*, Washington D.C., June 1986.
31. Mert M. Optimization of semi-empirical parameters in the FFA-Beddoes dynamic stall model. *FFA TN 1999-37*, 1999.
32. Haans W, Mikkelsen R. Airfoil models in the actuator line code assessed with near-wake measurements on a yawed rotor, *45th AIAA Aerospace Sciences Meeting and Exhibit*, Reno, Nevada, 8–11 January 2007.
33. Micallef D, Kloosterman M, Ferreira C, Sant T, van Bussel G. Validating BEM, direct and inverse free wake models with the MEXICO experiment, *48th AIAA conference, Jan 2010, paper 462*, Orlando, Florida.
34. Schepers J, Vermeer L. Een Engineering model voor Scheefstand op basis van Windtunnelmetingen. *ECN-CX—98-070*.
35. Burton T, Sharpe D, Jenkins N, Bossanyi E. *Wind Energy Handbook*. Wiley & Sons: West Sussex, England, 2001.
36. Snel H, Houwink R, van Bussel G, Bruining A. Sectional prediction of 3D effects for stalled flow on rotating blades and comparison with measurements, *Proceedings of the European Community Wind Energy Conference*, Lübeck-Travemünde, Germany, 8–12 March 1993; 395–399.
37. Chaviaropoulos P, Hansen M. Investigating three-dimensional and rotational effects on wind turbine blades by means of a quasi-3D Navier–Stokes solver. *Journal of Fluids Engineering* 2000; **122**: 330–336.